基于单幅散斑的 X 射线强度关联缺陷检测方法

杨海瑞[1,2,3]，谈志杰[1]，喻虹[1,3*]，潘雪娟[1]，韩申生[1,3]

[1]中国科学院上海光学精密机械研究所量子光学重点实验室，上海 201800；
[2]中国科学院大学，北京 100049；
[3]国科大杭州高等研究院，浙江 杭州 310024

摘要 采用预置散斑的 X 射线强度关联成像系统需要采集大量的散斑场，成像时间较长，而单幅散斑场信噪比低，难以单独用于图像重构。然而单幅散斑场中的空间分布信息包含一定的样品结构信息，可以用于样品缺陷快速检测。基于此，提出一种基于单幅预置散斑的缺陷检测方法，该方法将待检测样品探测散斑场与标准样品模拟散斑场的相关性作为样品缺陷的评价标准。同时基于该方法模拟 X 射线强度涨落二阶自关联检测光路，分析不同信噪比下探测散斑场分布的图像对比度对相关系数的影响。并对比多种细节增强方法，提高检测可靠性。最终结果表明，基于单幅散斑场的方法可以有效地进行样品的快速缺陷检测。

关键词 X 射线光学；图像增强；散斑自关联；缺陷检测；引导滤波

中图分类号 O434.19　　　　**文献标志码** A　　　　**DOI:** 10.3788/AOS221961

1 引 言

X 射线自 1895 年由伦琴发现以来，凭借其波长短、穿透性强等特点，成为分析宏观物体内部结构的有力工具，被广泛应用于生物分子成像和微纳结构检测等领域[1-5]。传统 X 射线成像技术，如吸收成像[1]、相衬成像[6-8]和相干衍射成像（CDI）[9-11]等，往往直接利用探测光场强度分布来获取样品相位与振幅信息。这些成像方法对 X 射线源的通量和相干性有较高的要求，难以实现小型化同时容易损坏样品。2016 年，Cheng 等[12-13]完成 X 射线傅里叶变换关联成像（FGI）验证实验，利用光场二阶关联特性提取样品的傅里叶强度谱并通过相位恢复算法得到样品强度与相位信息，这种方法对 X 射线光源空间相干性要求低，为小型化台式 X 射线显微成像提供可能。之后，该小组在 X 射线 FGI 领域针对空间复用[14]、非局域调制[15]、预置散斑场[16]等方面展开研究，研究结果表明，在低通量下使用预置散斑可实现高质量的成像。

利用预置散斑的强度涨落关联成像需要进行多组预置散斑照明，成像时间较长[17]。但是单幅探测散斑场分布所含信息，已经足够用来检测样品的部分特征，特别是直接用于快速的样品缺陷检测。由于低光通量情况下散斑场分布存在严重的散粒噪声等噪声[18]，直接用探测的单幅散斑场分析样品缺陷情况很容易出现偏差，所以需要对散斑场分布进行细节增强。图像细节增强常用方法有图像灰度变换、频域滤波、维纳滤波、图形形态学处理、非局域均值滤波（NL-Means）、三维块匹配滤波（BM3D）、小波变换和保边平滑的引导滤波等[19-28]。

本文提出一种利用单幅探测散斑场分布的缺陷检测方法，采用检测样品与标准样品散斑场分布的相关系数作为样品缺陷的评价标准。通过 X 射线强度涨落二阶自关联检测光路模拟能量为 1095 eV 的 X 射线检测，缺陷检测样品为十孔样品与电路样品。由于实验中散粒噪声等噪声会影响到散斑场的图像对比度，分析不同信噪比下散斑场分布的图像对比度对相关系数测量的影响。为提高该缺陷检测方法的可靠性，对比巴特沃斯高通滤波、维纳滤波、引导滤波等细节增强方法对相关系数检测的影响，从而选择合适的细节增强方法。

2 基本原理

2.1 强度涨落二阶自关联检测原理

传统的傅里叶关联成像的原理是计算探测光路与参考光路的光场强度涨落的互关联，从而得到样品的傅里叶强度谱[15]。而强度涨落二阶自关联的原理为计算单臂光场强度涨落的自关联，从而得到样品透过率函数平方的傅里叶强度谱，其原理如图 1 所示。入射

光先经过预置调制屏,沿预置光场传播距离 d_1 后通过样品,再传播距离 d_2 后被面阵 CCD 探测器接收,其强度分布为 $I(r)$。
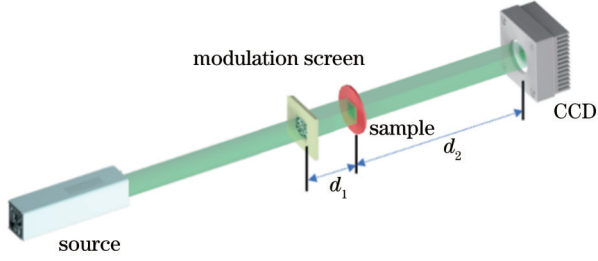

图 1　强度涨落二阶自关联原理图

Fig. 1　Schematic diagram of intensity fluctuation second-order autocorrection

探测光强涨落 $\Delta I(r)=I-\langle I\rangle$,其中,$\langle \cdot \rangle$ 表示系综平均,计算其光场强度涨落的二阶自关联[15]可得到:

$$\Delta G^{(2)}(r,r)=\langle \Delta I(r)\Delta I(r)\rangle\propto\left|\mathcal{F}\{t^2(r)\}\right|^2,\quad(1)$$

式中:$\mathcal{F}\{\cdot\}$ 表示傅里叶变换;$t(r)$ 为样品的透过率函数。多次测量后,通过系综平均计算探测光路光场强度涨落二阶自关联,可以得出样品透过率函数平方的傅里叶强度谱信息。

计算系综平均时,需要进行多组预置散斑照明测量,耗时长、重构速度慢。但单幅探测散斑场分布也携带样品大量的傅里叶频谱信息,足够用来进行快速的样品缺陷检测。

2.2　基于单幅散斑的检测处理流程

所提方法的检测处理流程如图 2 所示,具体流程如下:

1)设定图像旋转初始角度 $\theta=0°$ 与旋转分度 $\Delta\theta$。

2)输入标准样品,并对其旋转 θ,模拟仿真基于单幅预置散斑的光场传播,得到模拟散斑场分布。

3)通过对比探测散斑场图像对比度和模拟散斑场图像对比度,利用伽马变换[19]修正模拟散斑场分布的图像对比度。

图像对比度 δ 定义为

$$\delta=\sqrt{\frac{1}{M\times N}\sum_{i=1}^{M}\sum_{j=1}^{N}\left[\mathrm{image}(i,j)-\mu\right]^2},\quad(2)$$

式中:M 和 N 是图像横纵坐标的数量;$\mathrm{image}(i,j)$ 为 (i,j) 位置处的像素值;μ 是图像像素平均值。

4)以修正的模拟散斑场分布作为引导图,对探测散斑场分布进行引导滤波,并计算引导滤波结果与修正的模拟散斑场分布的相关系数。

修正的模拟散斑场分布为 I,探测散斑场分布为 P,引导滤波结果为 Q。引导滤波计算方法可看作局部窗口滤波:

$$Q_{ij}=\sum_j W_{ij}(I)P_{ij},\quad(3)$$

$$W_{ij}(I)=\frac{1}{n_k^2}\sum_{i,j\in w_k(i,j)}\left[1+\frac{(I_i-\mu_k)(I_j-\mu_k)}{\sigma_k^2+\varepsilon}\right],\quad(4)$$

式中:i 和 j 是像素的坐标;$W(\cdot)$ 是滤波的核函数;$w_{k(i,j)}$ 为以 (i,j) 为中心的局部窗口;μ_k 和 σ_k^2 分别为 $I_{i\in w_k}$ 的平均值与方差;n_k 为局部窗口 $w_{k(i,j)}$ 内的像素数;I_i 和 I_j 为两个相邻的像素点的值;ε 为正则项。

引导滤波结果 Q 与修正的模拟散斑场分布 I 的相关系数 ρ 的计算过程为

$$\rho(Q,I)=\frac{\sum_{i=1}^{n}(Q_i-\bar{Q})(I_i-\bar{I})}{\sqrt{\sum_{i=1}^{n}(Q_i-\bar{Q})^2}\sqrt{\sum_{i=1}^{n}(I_i-\bar{I})^2}}。\quad(5)$$

5)更新旋转角度,$\theta=\theta+\Delta\theta$,重复步骤 1)~4),直到 $\theta=360°$。最终输出随旋转角度变化的相关系数曲线,若相关系数 ρ 峰值低于 0.95,则认为样品存在缺陷。

3　仿真与结果分析

通过模拟 X 射线强度涨落二阶自关联检测光路生成预置光场,从而得到探测面散斑场分布。X 射线模拟能量为 1095 eV(Ga 的 L 线)。辐照二元调制屏的光源尺寸为 100 μm × 100 μm,近似平行光入射,二元调制屏的孔尺寸为 1 μm × 1 μm,调制屏的材质为 Au,相应的复折射率 $n=1-\delta+\mathrm{i}\beta$,$\delta=1.830\times10^{-3}$,$\beta=7.758\times10^{-3}$,调制模式由 NSGA-II 算法[16]生成,产生散斑场符合超瑞利分布。二元调制屏到样品平面距离 $d_1=8$ cm,样品平面到探测器距离 $d_2=1.92$ m。探测器探测尺寸为 3.84 mm × 3.84 mm,每个探测像素的尺寸为 15 μm × 15 μm。测试样品为两个,一个是十孔样品,另一个是电路样品,尺寸分别为 20 μm × 25 μm 和 15 μm × 15 μm,如图 3(a)、(b)所示。在模拟实验时,采用的缺陷样品如图 3(c)、(d)所示,其与标准样品图像的相关系数 ρ 为 0.90。对图 3(a)~(d)的 4 个样品分别进行探测光路每像素光子数为 1 的模拟实验,探测面探测散斑场分布分别为图 3(e)~(h)所示。

因为样品是随机角度插入光路的,所以需要进行样品的旋转角度匹配以进行缺陷检测。具体做法就是将标准样品旋转起来来模拟计算散斑场分布,从而构造不同的引导图用以匹配样品并确定旋转角度。在光路中插入旋转角度分别为 60° 与 103° 的十孔与电路样品,基于所得探测散斑场分布进行上述角度匹配,从而得到标准图旋转角度与相关系数 ρ 的角度匹配图,具体如图 4 所示。从图中可以看出,匹配的角度和样品缺陷检测的相关系数都与预设一致。由于测试的十孔标准样品为中心对称样品,因此,十孔样品的角度匹配图在 240° 位置也产生峰值。
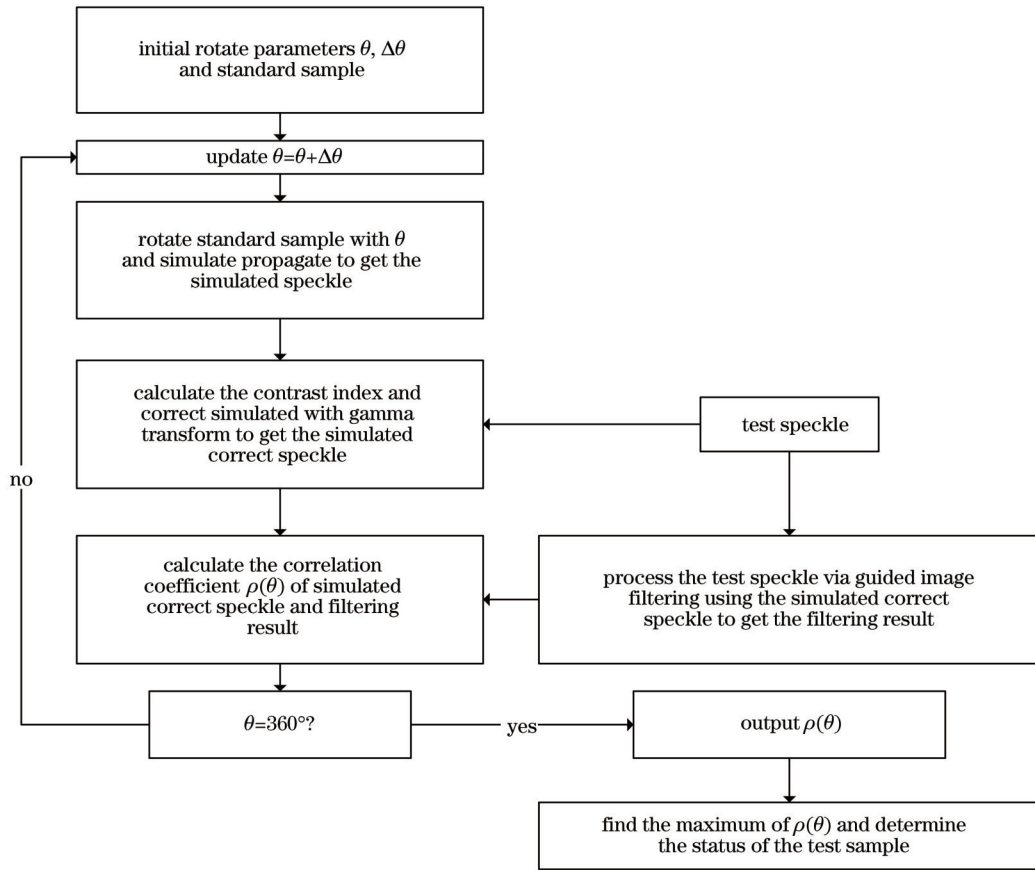
图 2 基于单幅散斑的信号处理流程图

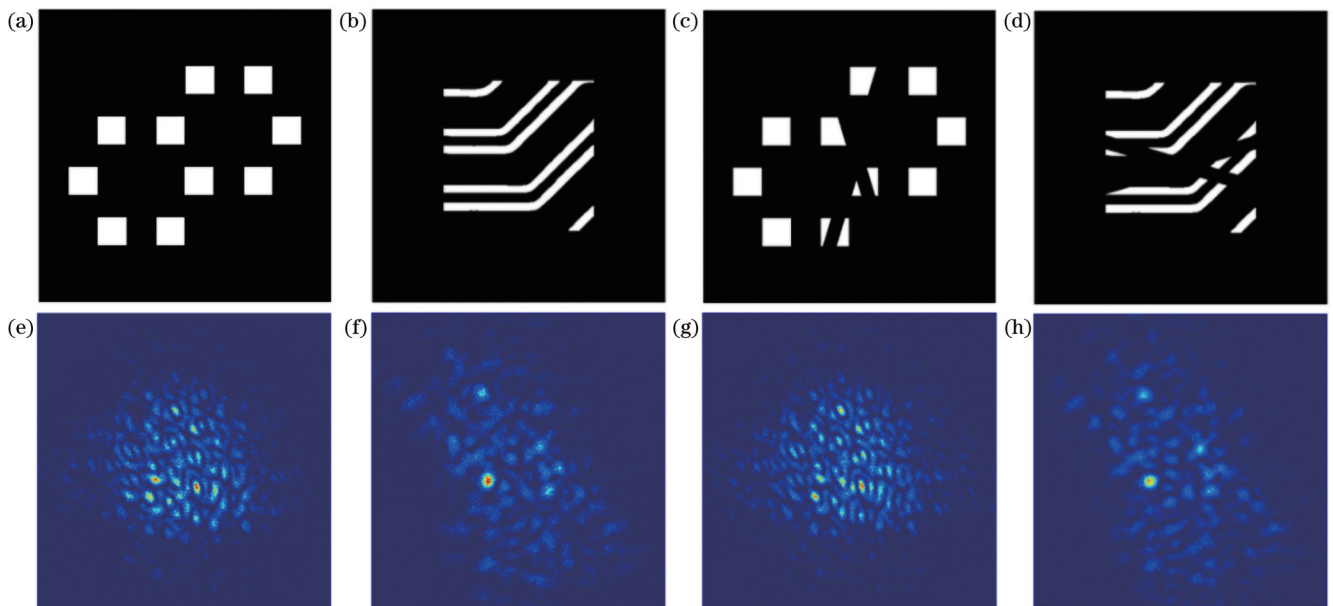Fig. 2 Signal processing flow chart using a single speckle pattern

图 3 检测样品与探测散斑场分布。(a)(e)十孔样品;(b)(f)电路样品;(c)(g)十孔缺陷样品;(d)(h)电路缺陷样品

Fig. 3 Test samples and detected speckle fields. (a)(e) 10-hole sample; (b)(f) circuit sample; (c)(g) 10-hole defected sample; (d)(h) circuit defected sample

3.1 图像对比度对相关系数的影响

实验时,由于探测的单幅散斑场分布往往存在严重的噪声且器探测存在直流背底,信号常常被噪声淹没,图像信噪比低使得图像对比度 δ 发生变化,导致探测散斑场分布的图像对比度 δ_{real} 与模拟散斑场的图像对比度 δ_{sim} 不一致。不同信噪比(R_{SN})下,图 3(a)的十
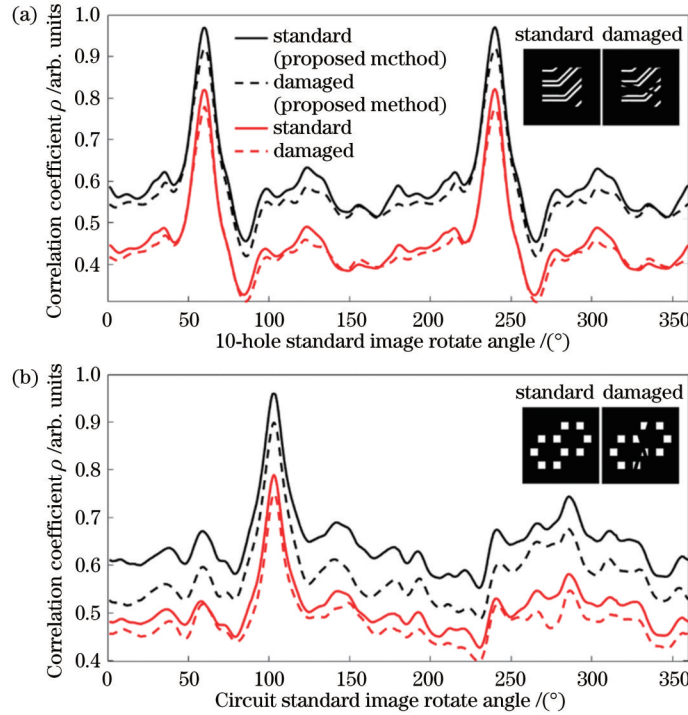
图 4　标准图旋转角度与相关系数 ρ 的角度匹配图。(a)十孔样品；(b)电路样品

Fig. 4　Angle matching diagram of the rotation angle of the standard image and the correlation coefficient ρ. (a) 10-hole sample;
(b) circuit sample

孔样品的散斑场分布如图 5 所示，不同信噪比通过添加高斯白噪声实现，其图像对比度大小随不同方差的噪声加入发生变化。

　　针对图像对比度 δ，对模拟散斑场分布进行伽马变换修正，探测散斑场分布与模拟散斑场分布的相关系数 ρ 会随图像对比度修正系数 γ 发生变化，如图 6 所示。从图 6 可以看出，低信噪比散斑场在合适的伽马变换修正时，相关系数 ρ 存在最大值，其最大值是所提样品缺陷检测方法能将相关系数提高到的"上限"，如图 6 中虚线所示。

3.2　散斑场细节增强方法对比

　　对图 3(e)～(h)分别进行巴特沃斯高通滤波、维纳滤波和以各自标准样品的模拟散斑场分布为引导图的引导滤波。以图 3(g)中的探测散斑场分布为例，其巴特沃斯高斯滤波结果如图 7(a)所示，维纳滤波结果如图 7(b)所示，引导滤波结果如图 7(c)所示。从图中可以看出，巴特沃斯高通滤波可以增强高频信号，但是低频信号会有很严重的丢失，维纳滤波与引导滤波的平滑背景和保持细节方面都很有效。3 个滤波结果、引导图散斑场分布结果与图 3(g)中的探测面散斑场分布在 $x=0$ 处的横截面如图 7(d)所示。引导滤波结果在绝大多数细节上与维纳滤波结果相似，但是与标准样品的模拟散斑场分布存在不一致的细节，滤波结果会不同于探测散斑场分布，也就是说，样品缺陷所对应的探测细节会被标准样品的模拟散斑场分布的引导作用而弱化甚至消失。因此，引导滤波方法具有更好的缺陷检测效果。同时，引导滤波能够过滤信噪比更低的信号，避免误判。

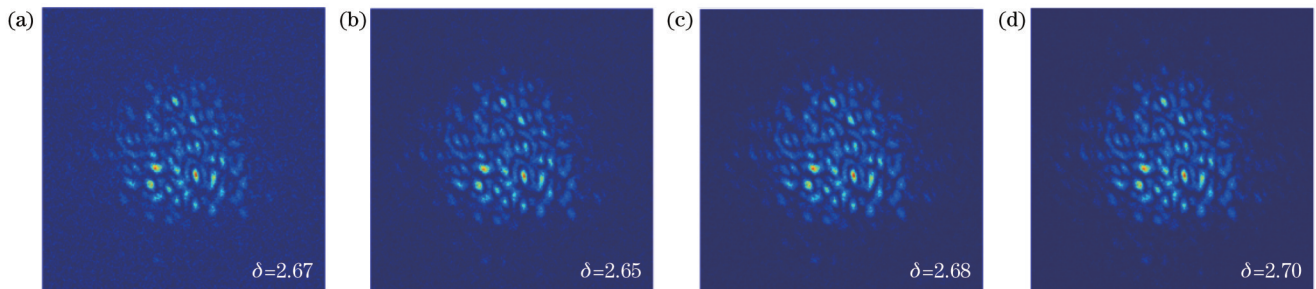图 5　不同信噪比的探测散斑场分布。(a) $R_{SN}=5\,dB$；(b) $R_{SN}=10\,dB$；(c) $R_{SN}=15\,dB$；(d) $R_{SN}=20\,dB$

Fig. 5　Defected speckle fields under different signal-to-noise ratios. (a) $R_{SN}=5\,dB$; (b) $R_{SN}=10\,dB$; (c) $R_{SN}=15\,dB$; (d) $R_{SN}=20\,dB$
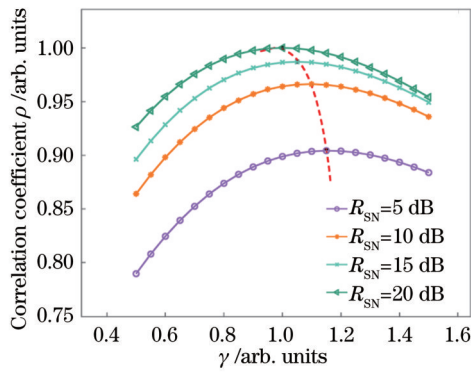
图 6 不同信噪比时，相关系数 ρ 与探测散斑场图像对比度修正系数 γ 的变化图

Fig. 6 the variation of correlation coefficient ρ and detected speckle field's image contrast adjust coefficient γ with different signal-to-noise ratios

滤波处理结果与标准样品的模拟散斑场分布的相关系数 ρ 如表1所示。引导滤波对于和引导图相似的图像处理效果更佳，这样的特性能提高检测的准确性。标准十孔样品与电路样品的探测散斑场分布通过引导滤波的细节增强后其相关系数分别为 0.96 和 0.97，存在缺陷的十孔样品与电路样品的相关系数分别为 0.91 和 0.90。

4 结 论

基于 X 射线强度涨落自关联原理和单幅预置散斑场构建了样品快速缺陷检测方法。同时，基于该方法模拟 X 射线强度涨落二阶自关联检测光路，对十孔和

表 1 滤波处理结果与模拟散斑场分布的相关系数 ρ

Table 1 Correlation coefficient ρ of the processed results and the simulated speckle field

Detail enhancement measure	Standard 10-hole sample	Defected 10-hole sample	Standard circuit sample	Defected circuit sample
	Correlation coefficient ρ /arb. units			
Unprocessed	0.93	0.88	0.92	.84
High-pass filtering	0.70	0.64	0.78	0.71
Wiener filtering	0.95	0.90	0.95	0.88
Guided image filtering	0.96	0.91	0.97	0.90

电路样品进行模拟缺陷检测，均可以得到准确的旋转匹配角度与缺陷检测结果。考虑实际情况中不同信噪比下图像会有不同的对比度，对比度的变化会影响到相关系数的测量值，通过伽马变换修正对比度可以提高细节增强时相关系数的"上限"，从而提高检测准确性。通过对比不同的细节增强方法发现，当利用引导滤波方法细节增强探测散斑场分布时，与标准图一致的细节将被增强，与标准图不一致的细节将被平滑，可以将标准样品的相关系数测量值提高到 0.95 以上，而具有缺陷的样品相关系数测量值无法提高到这样的水平，这样的特性极大地提高了此样品缺陷检测方法的可靠性。该方法从原理上并不需要很好的相干源，为小型化 X 射线检测在半导体器件、集成电路、高性能材料等方面应用提供了可能。
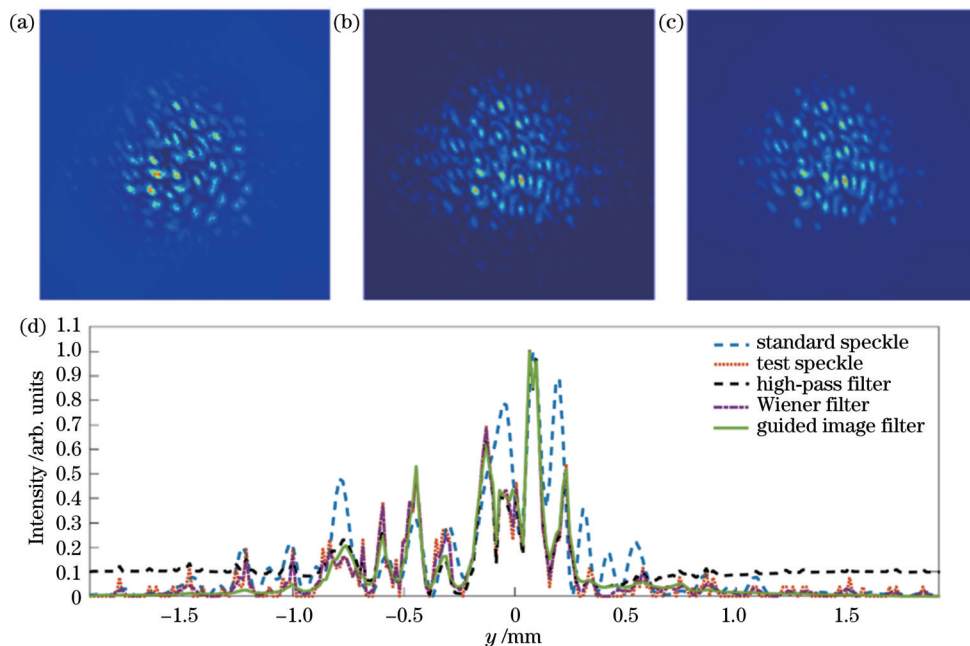

图 7 细节增强结果。(a)高通滤波处理结果；(b)维纳滤波处理结果；(c)引导滤波处理结果；(d)各种滤波结果、标准样品散斑场分布与图3(g)中的探测散斑场分布在 $x=0$ 处的横截面

Fig. 7 Detail enhancement results. (a) High-pass filtering result; (b) Wiener filtering result; (c) guided filtering result; (d) the cross-section of various filtering results, standard speckle, and test speckle in Fig. 3(g), when $x=0$

参 考 文 献

[1] Rroentgen W C. On a new kind of rays[J]. Science, 1896, 3(59): 227-231.

[2] Fleury B, Cortes-Huerto R, Taché O, et al. Gold nanoparticle internal structure and symmetry probed by unified small-angle X-ray scattering and X-ray diffraction coupled with molecular dynamics analysis[J]. Nano Letters, 2015, 15(9): 6088-6094.

[3] Kosynkin D V, Higginbotham A L, Sinitskii A, et al. Longitudinal unzipping of carbon nanotubes to form graphene nanoribbons[J]. Nature, 2009, 458(7240): 872-876.

[4] 黎森, 姚童, 王玺, 等. X射线晶体衍射谱仪理论及应用[J]. 光学学报, 2022, 42(11): 1134008.
Li M, Yao T, Wang X, et al. X-ray crystal diffraction spectrometer: theory and application[J]. Acta Optica Sinica, 2022, 42(11): 1134008.

[5] 谈志杰, 李晴宇, 喻虹, 等. X射线及粒子关联成像技术研究进展[J]. 激光与光电子学进展, 2021, 58(10): 1011008.
Tan Z J, Li Q Y, Yu H, et al. Progress on ghost imaging with X-ray and particles[J]. Laser & Optoelectronics Progress, 2021, 58(10): 1011008.

[6] Davis T J, Gao D, Gureyev T E, et al. Phase-contrast imaging of weakly absorbing materials using hard X-rays[J]. Nature, 1995, 373(6515): 595-598.

[7] Endrizzi M. X-ray phase-contrast imaging[J]. Nuclear Instruments and Methods in Physics Research Section A: Accelerators, Spectrometers, Detectors and Associated Equipment, 2018, 878: 88-98.

[8] Takeda T. Phase-contrast and fluorescent X-ray imaging for biomedical researches[J]. Nuclear Instruments and Methods in Physics Research Section A: Accelerators, Spectrometers, Detectors and Associated Equipment, 2005, 548(1/2): 38-46.

[9] Mancuso A P, Yefanov O M, Vartanyants I A. Coherent diffractive imaging of biological samples at synchrotron and free electron laser facilities[J]. Journal of Biotechnology, 2010, 149(4): 229-237.

[10] Jiang H D. Cryo-coherent diffractive imaging of biological samples with X-ray free-electron lasers[J]. Acta Crystallographica. Section A, Foundations and Advances, 2016, 72(2): 177-178.

[11] Nishino Y, Takahashi Y, Imamoto N, et al. Three-dimensional visualization of a human chromosome using coherent X-ray diffraction[J]. Physical Review Letters, 2009, 102(1): 018101.

[12] Cheng J, Han S S. Incoherent coincidence imaging and its applicability in X-ray diffraction[J]. Physical Review Letters, 2004, 92(9): 093903.

[13] Yu H, Lu R H, Han S S, et al. Fourier-transform ghost imaging with hard X-rays[J]. Physical Review Letters, 2016, 117(11): 113901.

[14] Zhu R G, Yu H, Lu R H, et al. Spatial multiplexing reconstruction for Fourier-transform ghost imaging via sparsity constraints[J]. Optics Express, 2018, 26(3): 2181-2190.

[15] Tan Z J, Yu H, Lu R H, et al. Non-locally coded Fourier-transform ghost imaging[J]. Optics Express, 2019, 27(3): 2937-2948.

[16] 陈倩, 喻虹, 谈志杰, 等. X光超瑞利散斑场傅里叶变换关联成像模拟研究[J]. 光学学报, 2021, 41(19): 1934001.
Chen Q, Yu H, Tan Z J, et al. Simulation research on X-ray Fourier-transform ghost imaging using super-Rayleigh speckle field[J]. Acta Optica Sinica, 2021, 41(19): 1934001.

[17] Liu S Y, Liu Z T, Hu C Y, et al. Spectral ghost imaging camera with super-Rayleigh modulator[J]. Optics Communications, 2020, 472: 126017.

[18] 李晴宇, 谈志杰, 喻虹, 等. X射线傅里叶关联成像中的康普顿散射噪声研究(特邀)[J]. 红外与激光工程, 2021, 50(12): 20210734.
Li Q Y, Tan Z J, Yu H, et al. Research on Compton scattering noise in the X-ray Fourier-transform ghost imaging(Invited)[J]. Infrared and Laser Engineering, 2021, 50(12): 20210734.

[19] Baidoo E, Kwesi K A. Implementation of gray level image transformation techniques[J]. International Journal of Modern Education and Computer Science, 2018, 10(5): 44-53.

[20] Wiener N. Response of a non-linear device to noise[D]. Massachusetts: Massachusetts Institute of Technology, 1942.

[21] Ram I, Elad M, Cohen I. Image denoising using NL-means via smooth patch ordering[C]//2013 IEEE International Conference on Acoustics, Speech and Signal Processing, May 26-31, 2013, Vancouver, BC, Canada. New York: IEEE Press, 2013: 1350-1354.

[22] Dabov K, Foi A, Katkovnik V, et al. BM3D image denoising with shape-adaptive principal component analysis[EB/OL]. [2022-10-09]. https://hal.inria.fr/inria-00369582/.

[23] He K M, Sun J, Tang X O. Guided image filtering[M]// Daniilidis K, Maragos P, Paragios N. Computer vision-ECCV 2010. Lecture notes in computer science. Heidelberg: Springer, 2010, 6311: 1-14.

[24] Hao H Q, Liu M, Xiong P, et al. Multi-lead model-based ECG signal denoising by guided filter[J]. Engineering Applications of Artificial Intelligence, 2019, 79: 34-44.

[25] Hao S J, Pan D R, Guo Y R, et al. Image detail enhancement with spatially guided filters[J]. Signal Processing, 2016, 120: 789-796.

[26] Liang Z F, Liu H Z, Zhang B T, et al. Real-time hardware accelerator for single image haze removal using dark channel prior and guided filter[J]. IEICE Electronics Express, 2014, 11(24): 20141002.

[27] Kou F, Chen W H, Wen C Y, et al. Gradient domain guided image filtering[J]. IEEE Transactions on Image Processing, 2015, 24(11): 4528-4539.

[28] 裴佩佩, 杨艳春, 党建武, 等. 基于滚动引导滤波器和卷积稀疏表示的红外与可见光图像融合方法[J]. 激光与光电子学进展, 2022, 59(12): 1210001.
Pei P P, Yang Y C, Dang J W, et al. Infrared and visible image fusion method based on rolling guidance filter and convolution sparse representation[J]. Laser & Optoelectronics Progress, 2022, 59(12): 1210001.

X-Ray Intensity Correlation Defect Detection Using a Single Speckle Pattern

Yang Hairui[1,2,3], Tan Zhijie[1], Yu Hong[1,3*], Pan Xuejuan[1], Han Shensheng[1,3]

[1]*Key Laboratory for Quantum Optics, Shanghai Institute of Optics and Fine Mechanics, Chinese Academy of Sciences, Shanghai* 201800, *China*;
[2]*University of Chinese Academy of Sciences, Beijing* 100049, *China*;
[3]*Hangzhou Institute for Advanced Study, University of Chinese Academy of Sciences, Hangzhou* 310024, *Zhejiang, China*

Abstract

Objective　　X-ray is a powerful tool to analyze the internal structure of macroscopic objects and has been widely used in many fields, such as biomolecular imaging and micro/nanostructure detection. Traditional X-ray analysis techniques often have high requirements for light flux and coherence, which are difficult to be applied in a table-top source and thus limit their application. X-ray Fourier-transform ghost imaging (XFGI) has a low requirement for spatial coherence and enables table-top X-ray microscopic detection and imaging. In recent years, researchers have focused on spatial multiplexing, non-local modulation, preset speckle field, and other aspects in the field of XFGI, and it is shown that high-quality imaging can be achieved by using preset speckle patterns at low flux. XFGI via preset speckle patterns needs to measure a mass of speckle fields, and imaging consumes time. A single speckle field has a low signal-to-noise ratio and cannot be used to retrieve the image independently. However, certain sample structure information can be extracted from the spatial distribution of the single speckle field, which can be employed to realize rapid sample defect detection. We aim to propose a method for sample defect detection by using a single speckle pattern, which will be helpful for micro/nanostructure detection and analysis.

Methods　　In this paper, a defect detection method based on speckle field distribution by single detection is proposed, and the correlation coefficient between the detected speckle field distribution of test samples and standard samples is used as the evaluation function for sample defect detection. The second-order autocorrelation detection of intensity fluctuation is simulated with the energy of 1095 eV, and defect detection samples have two types: samples with ten holes and circuit samples. Since experimental noise, such as shot noise, can affect the image contrast of the speckle field, the effect of speckle contrast is analyzed under different signal-to-noise ratios. To improve the reliability of this defect detection method, this paper compares the influence of different detail enhancement methods, such as Butterworth high-pass filtering, Wiener filtering, and guided image filtering, on the correlation coefficient detection, so as to select the appropriate detail enhancement method.

Results and Discussions　　Samples with ten holes and circuit samples that have rotation angles of 60° and 103°, respectively, are inserted into the optical path to get the detected speckle field distributions and then process the defect detection (Fig. 2). The matching angle and the correlation coefficient of defect detection results are consistent with the presupposition (Fig. 4). For image contrast, this paper corrects simulated speckle field distributions by gamma transform, and the correlation coefficient between detected speckle field distribution and simulated speckle field distribution will change with the image contrast correction coefficient. When the speckle field with a low signal-to-noise ratio is corrected by appropriate gamma transform, the correlation coefficient has a maximum value, which is the upper limit that this sample defect detection method can raise the correlation coefficientto (Fig. 6). For different detail enhancement methods, the results of guided image filtering are similar to Wiener filtering results in most details. However, for details inconsistent with the simulated speckle field distribution of the standard sample, the filtering results will be different from the detected speckle field distribution. The detection details corresponding to the sample defects will be weakened or even disappeared under the guidance of the simulated speckle field distribution of the standard samples. Therefore, the guided image filtering method has a better defect detection effect (Fig. 7 and Table 1). At the same time, guided image filtering can smooth signals with a lower signal-to-noise ratio to avoid the misjudgment of detection (Fig. 7).

Conclusions　　In this paper, based on the autocorrelation principle of intensity fluctuation, a fast defect detection method is developed by using a single preset speckle pattern. At the same time, based on this method, the second-order autocorrelation detection optical path of X-ray intensity fluctuation is simulated, and the defect detection of samples with ten holes and circuit samples is simulated. The accurate rotation matching angle and defect detection results can be obtained. In view of the actual situation, the images will have different contrasts under different signal-to-noise ratios, and the change in the contrast will affect the reduction of the measured value of the correlation coefficient. The gamma

transform can correct the contrast and improve the upper limit of the correlation coefficient when the details are enhanced, so as to improve the detection accuracy. By comparing different detail enhancement methods, this paper also finds that the details consistent with the standard image will be enhanced, and those inconsistent with the standard image will be smoothed when the guided image filtering method is used to process the detected speckle field distribution. The measured correlation coefficient of the standard samples can be increased to more than 0.95. However, the measured value of the correlation coefficient of samples with defects cannot be improved to such a level, and this property greatly improves the reliability of this sample defect detection method. In principle, this method does not require a coherent source, which makes it possible for applying table-top X-ray detection in semiconductor devices, integrated circuits, high-performance materials, and other aspects.